# Segmentation and analysis of 3D zebrafish cell image data

Karol Mikula
Mariana Remešíková
and Olga Stašová
Slovak University of Technology
Bratislava, Slovakia
mikula@math.sk, remesikova@math.sk
stasova@math.sk

Nadine Peyriéras
CNRS-EPSN
Gif sur Yvette, France
nadine.peyrieras@inaf.cnrs-gif.fr

***Abstract*—In this paper, we describe methods designed to segment objects from 3D cell nuclei and cell membrane images and we point out several possible applications in analysis of the zebrafish cell image data. We show how we can segment the cell nuclei, the inner boundaries of the cells, the outer boundary of an organism and the intercellular borders. We also present a method for detection of approximate nuclei centers that is a necessary preliminary step for the segmentation. All methods that we mention are based on numerical solution of partial differential equations. We describe all mathematical models and we sketch the principles of the time and space discretization. The explanation of all methods is accompanied by illustrations and suggestions of applications in biology.**

## I. Introduction

The main goal of this paper is to propose several PDE methods designed to extract objects from 3D zebrafish cell images. Our research was motivated by the idea of bringing in a set of reliable techniques that would enable us to analyze the cell images – determine the number of cells, evaluate their shapes, measure some important quantities like the surface or volume, detect various cell structures, evaluate the global and local characteristics of the whole organism, e.g. the density of cells or location of cell divisions. Such analysis could be further extended to comparison of different individuals or to analysis of 4D data, i.e. the time evolution of an organism.

The images that we are dealing with represent the evolution of the zebrafish embryo and they were obtained by a confocal microscope that scanned simultaneously the cell nuclei and cell membrane channel. All images are three-dimensional, they are represented by the grey-level scale and they usually contain several hundreds to several thousands of cells – a number that would be impossible to analyze manually, especially if we have to deal with long time series representing various stages of embryogenesis. An example of the data is shown in Fig. 1.

The presented types of images can be used to extract various objects – individual cells, cell structures (at later stages of embryogenesis) or the surface of the organism. In this paper, we describe methods for segmentation of the cell nuclei, the inner cell boundaries, the so called intercellular skeleton (the cell contact surface) and the embryo surface. The segmentation methods, in order to start from an appropriate initial condition, require the approximate positions of all cells. Therefore, before explaining the segmentation algorithms, we present a method for detection of approximate cell nuclei centers [7].

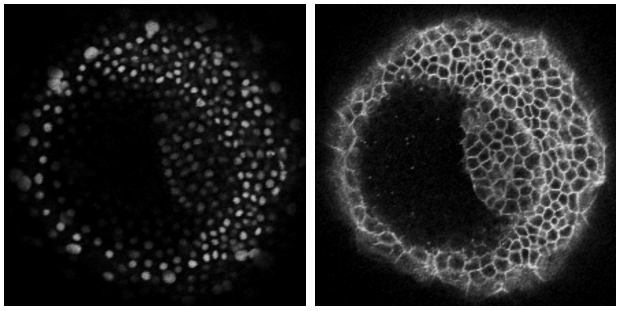

Fig. 1. Zebrafish embryo image in a 2D slice view. Left, the image of cell nuclei, right, the cell membranes.

The center detection technique is represented by a level set equation for advective motion in normal direction with curvature term. The segmentation of the cell nuclei, the inner cell boundaries and the embryo surface is realized by an advection-diffusion type model, the so called generalized subjective surface equation [6], [10], [11], [13], [15]. The intercellular borders are segmented by an advective version of the generalized subjective surface model. The velocity field in this equation is given by the gradient of the signed distance function to the inner cell borders that is computed by solving the time relaxed eikonal equation [2]. These methods compose a powerful set of cell image analysis techniques and they have been extensively tested and successfully applied, cf e.g. [1]–[3], [7], [9], [10], [15]. Since the numerous experiments pointed out also some practical difficulties and possibilities of efficiency improvement, we decided to modify the numerical approaches described in the cited works. The schemes presented in this paper are based on the following principles. The time discretization of the time relaxed eikonal equation and the advective subjective surface model is explicit while the center detection equation and generalized subjective surface model, since they contain nonlinear curvature terms, are discretized by the semi-implicit approach. As for the space discretiza-

tion, the advective term in the subjective surface models is approximated by applying the upwind principle. The center detection equation and the eikonal equation contain the term that represents motion of level sets in normal direction. Here we apply the Rouy-Tourin scheme [12]. The discretization of the curvature terms is based on the finite volume technique.

## II. The cell image processing algorithms

In this section, we describe the mathematical models, we explain the principles of their numerical approximation and we present some illustrative examples. Let us note that before any of the methods can be applied, the images have to be preprocessed by some denoising algorithm since a certain level of noise is always present due to the limits of the staining and scanning techniques. For our purposes, we applied the geodesic mean curvature flow method [4], [5], [8] that was chosen from several PDE methods after thorough testing, cf [9]. From now on, we will use the notation $u^0_{N_f} : \Omega \to R$, where $\Omega$ is a 3D rectangular domain, for the intensity function representing the filtered nuclei image and $u^0_{M_f}$ for the filtered membrane image.

### A. The discretization notation

Before we start explaining the algorithms, we establish some common notation. All equations are discretized uniformly in time and space, with $\tau_C$, $h_C$, $\tau_S$, $h_S$, $\tau_D$, $h_D$ and $\tau_A$, $h_A$ being the time and space steps for the center detection, generalized subjective surface segmentation, computation of the distance function and advective subjective surface segmentation, respectively. The space discretization is based on the finite volume principle where the volumes of the mesh $\mathcal{T}_h$ are indetified with the voxels of the 3D image and any volume $V_{ijk}$, $i = 1 \dots N_1$, $j = 1 \dots N_2$, $k = 1 \dots N_3$, is represented by a cube with side length corresponding to the space step. Let $c_{ijk}$ be the barycenter of $V_{ijk}$. For all volumes $V_{ijk}$, we define three index sets:

- $N_{ijk} = \{(p,q,r); p,q,r \in \{-1,0,1\}, |p|+|q|+|r| = 1\}$
- $P_{ijk} = \{(p,q,r); p,q,r \in \{-1,0,1\}, |p|+|q|+|r| = 2\}$
- $I_{ijk} = \{(1,0,0),(0,1,0),(0,0,1)\}$

For any $(p,q,r) \in N_{ijk}$, the faces of the finite volume $V_{ijk}$ are denoted by $e^{pqr}_{ijk}$ with normal $\nu^{pqr}_{ijk}$ and barycenter $x^{pqr}_{ijk}$. For $(p,q,r) \in P_{ijk}$, $y^{pqr}_{ijk}$ denotes the midpoints of the voxel edges. The approximate value of the model solution $u$ in $c_{ijk}$ at time step $n$ is denoted by $u^n_{ijk}$, the values of $u$ at $x^{pqr}_{ijk}$ and $y^{pqr}_{ijk}$ at time step $n-1$ are denoted by (omitting the time index) $u^{pqr}_{ijk}$, $(p,q,r)$ belonging to the corresponding index set. The described mesh is sketched in Fig. 2.

### B. Cell nuclei center detection

The center detection process is represented by the equation [7]

$$u_t - \delta|\nabla u| - \mu|\nabla u|\nabla \cdot \left(\frac{\nabla u}{|\nabla u|}\right) = 0 \qquad (1)$$

coupled with the zero Neumann boundary condition and the initial condition $u_0 = u^0_{N_f}$, solved in the domain $\Omega \times [0, T_C]$.

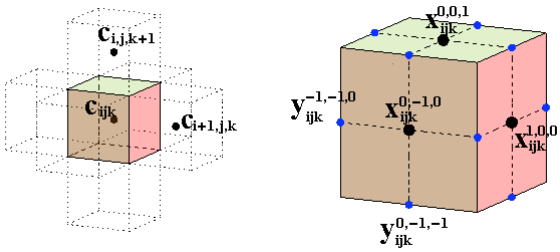


Fig. 2. The finite volume mesh.

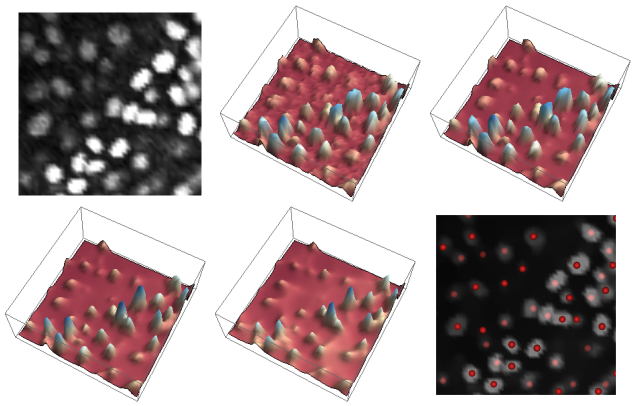

Fig. 3. The nuclei center detection process. Top left, 2D slice of the nuclei image. Top middle, the corresponding intensity function. Top right, intensity function of the filtered data. Bottom left and middle, the intensity function after 5 and 15 steps of the evolution given by (1). Bottom right, the corresponding centers constructed after 5 time steps (optimal stopping time) of the evolution.

This model represents the advective level set motion in normal direction regularized by curvature, i.e. the motion with the velocity $V = \delta + \mu k$ where $\delta$ and $\mu$ are constants and $k$ is the mean curvature. The evolving level sets are the image intensity level sets corresponding to the objects in the nuclei image. During this evolution, all level sets are shrinking and finally they disappear, while the level sets with a relatively small diameter representing the noise structures disappear quickly and the ones with larger diameter corresponding to cell nuclei are observable in a much longer time scale. In other words, we can observe decreasing of the number of the local maxima of $u$ that is stabilized when the spurious structures disappear. At this point, we stop the process and the positions of local maxima of $u$ will represent the approximate cell nuclei centers (see Fig. 3).

In order to discretize (1) in time, we apply the semi-implicit approach that guarantees the unconditional stability of the curvature term. We get

$$\frac{u^n - u^{n-1}}{\tau_C} - \delta|\nabla u^{n-1}| - \mu|\nabla u^{n-1}|\nabla \cdot \left(\frac{\nabla u^n}{|\nabla u^{n-1}|}\right) = 0\,. \qquad (2)$$

After, applying the finite volume technique, we integrate (2)

over $V_{ijk}$. We obtain

$$\int\limits_{V_{ijk}} \frac{u^n - u^{n-1}}{\tau_C}\,dx - \int\limits_{V_{ijk}} \delta|\nabla u^{n-1}|\,dx - \int\limits_{V_{ijk}} \mu|\nabla u^{n-1}|\nabla\cdot\left(\frac{\nabla u^n}{|\nabla u^{n-1}|}\right)\,dx = 0\,, \tag{3}$$

where the time derivative term can be approximated by

$$\int\limits_{V_{ijk}} \frac{u^n - u^{n-1}}{\tau_C}\,dx \approx h_C^3 \frac{u^n_{ijk} - u^{n-1}_{ijk}}{\tau_C}\,. \tag{4}$$

The second term contains the absolute value of the gradient $|\nabla u^{n-1}|$ that can be discretized by the Rouy-Tourin scheme [12]. Let us define for any $(p,q,r) \in N_{ijk}$

$$D^{pqr}_{ijk} = \left(\min\left(u^{n-1}_{i+p,j+q,k+r} - u^{n-1}_{ijk}, 0\right)\right)^2 \tag{5}$$

and further for any $(p,q,r) \in I_{ijk}$

$$M^{pqr}_{ijk} = \max\left(D^{-p,-q,-r}_{ijk}, D^{p,q,r}_{ijk}\right)\,. \tag{6}$$

Then we get the approximation

$$|\nabla u^{n-1}| \approx \frac{1}{h_C}\sqrt{M^{100}_{ijk} + M^{010}_{ijk} + M^{001}_{ijk}}\,. \tag{7}$$

In order to approximate the integral of the curvature term in (3), we first approximate the values of $u^{n-1}$ in the midpoints $y^{pqr}_{ijk}$, $(p,q,r) \in P_{ijk}$, of the voxel edges

$$\begin{aligned} u^{pq0}_{ijk} &= (u^{n-1}_{ijk} + u^{n-1}_{i+p,j,k} + u^{n-1}_{i,j+q,k} + u^{n-1}_{i+p,j+q,k})/4\,,\\ u^{p0r}_{ijk} &= (u^{n-1}_{ijk} + u^{n-1}_{i+p,j,k} + u^{n-1}_{i,j,k+r} + u^{n-1}_{i+p,j,k+r})/4\,,\\ u^{0qr}_{ijk} &= (u^{n-1}_{ijk} + u^{n-1}_{i,j+q,k} + u^{n-1}_{i,j,k+r} + u^{n-1}_{i,j+q,k+r})/4. \end{aligned} \tag{8}$$

Now we denote by $\nabla^{pqr}u^{n-1}_{ijk}$ the approximation of the gradient in the barycenter $x^{pqr}_{ijk}$ of the face $e^{pqr}_{ijk}$, $(p,q,r) \in N_{ijk}$, of the voxel $V_{ijk}$. Using this notation, we can define

$$\nabla^{p00}u^{n-1}_{ijk} = \left(\frac{p(u^{n-1}_{i+p,j,k} - u^{n-1}_{ijk})}{h_C}, \frac{u^{p10}_{ijk} - u^{p,-1,0}_{ijk}}{h_C}, \frac{u^{p01}_{ijk} - u^{p,0,-1}_{ijk}}{h_C}\right) \tag{9}$$

and analogously we define the approximations $\nabla^{0q0}u^{n-1}_{ijk}$, $\nabla^{00r}u^{n-1}_{ijk}$. Finally we set

$$Q^{pqr;n-1}_{ijk} = |\nabla^{pqr}u^{n-1}_{ijk}|, \quad \bar{Q}^{n-1}_{ijk} = \frac{1}{6}\sum_{N_{ijk}} |\nabla^{pqr}u^{n-1}_{ijk}|. \tag{10}$$

This leads to the following approximation

$$\int\limits_{V_{ijk}} \mu|\nabla u^{n-1}|\nabla\cdot\left(\frac{\nabla u^n}{|\nabla u^{n-1}|}\right)\,dx \approx \mu\bar{Q}^{n-1}_{ijk}\sum_{N_{ijk}}\int\limits_{e^{pqr}_{ijk}} \frac{\nabla u^n}{|\nabla u^{n-1}|}\nu^{pqr}_{ijk}\,d\gamma \;\approx\; \mu h_C\bar{Q}^{n-1}_{ijk}\sum_{N_{ijk}} \frac{u^n_{i+p,j+q,k+r} - u^n_{ijk}}{Q^{pqr;n-1}_{ijk}}. \tag{11}$$

At the end, let us note that in practical implementations the terms $Q^{pqr;n-1}_{ijk}$, $\bar{Q}^{n-1}_{ijk}$ are replaced by their regularized equivalents $Q^{pqr;n-1}_{\varepsilon,ijk} = \sqrt{\varepsilon^2 + |\nabla^{pqr}u^{n-1}_{ijk}|^2}$, $\bar{Q}^{n-1}_{\varepsilon,ijk} = \sqrt{\varepsilon^2 + \frac{1}{6}\sum_{N_{ijk}}|\nabla^{pqr}u^{n-1}_{ijk}|^2}$.

### C. Generalized subjective surface segmentation

This segmentation technique can be used to segment the cell nuclei, the inner cell boundaries and the embryo surface. The process is represented by the following model [6], [10], [13], [15]

$$u_t - w_a\nabla g\cdot\nabla u - w_d g|\nabla u|\nabla\cdot\left(\frac{\nabla u}{|\nabla u|}\right) = 0\,, \tag{12}$$

solved in $\Omega\times[0,T_s]$, where $u$ is the evolving function and we consider the zero Dirichlet boundary condition on $\partial\Omega$. The constants $w_a$ and $w_d$ are the coefficients (weights) of advection and diffusion. The function $g$ is the so called edge detector and it is of the form

$$g(s) = \frac{1}{1+Ks^2}\,, \qquad K \geq 0. \tag{13}$$

It is applied to the gradient of the filtered image additionally smoothed by the Gaussian kernel with a small variance $\sigma$ ($g = g(|\nabla u^0_\sigma|)$, $u^0_\sigma = G_\sigma * u^0_{N_f}$ in case of nuclei segmentation and $u^0_\sigma = G_\sigma * u^0_{M_f}$ in case of cell boundary and embryo surface segmentation). The essential property of this function is that its negative gradient points towards the edges in the image. In some applications, the efficiency of the method can be improved if we set $g(s) = f\left(1/(1+Ks^2)\right)$ where $f$ is an appropriate function that preserves the edge detecting properties.

The construction of the initial condition depends on the object that we want to segment. In case of the nuclei segmentation, we use a function whose compact support is localized in the neighborhood of the approximate nucleus center and it covers the whole nucleus. In case of inner cell boundary segmentation, the compact support of the function should be situated inside the cell. If we want to segment the embryo surface, the compact support should cover the whole embryo or its part that is visible in the image, see [1] for details.

The time discretization of (12) is again semi-implicit

$$\frac{u^n - u^{n-1}}{\tau_S} - w_a\nabla g\cdot\nabla u^{n-1} - w_d g|\nabla u^{n-1}|\nabla\cdot\frac{\nabla u^n}{|\nabla u^{n-1}|} = 0\,. \tag{14}$$

After integrating (14) over $V_{ijk}$, the integral of the time derivative term is approximated according to (4). In order to discretize the other to terms, recalling (8) and (9) we define

$$g_{ijk} = g\left(\frac{1}{6}\sum_{N_{ijk}}|\nabla^{pqr}u^0_{\sigma;ijk}|\right).$$

The advection term is approximated by the upwind principle. For all $(p,q,r) \in I_{ijk}$, we define the differences

$$D^{pqr}_{ijk}g = (g_{i+p,j+q,k+r} - g_{i-p,j-q,k-r})/(2h_S). \tag{15}$$

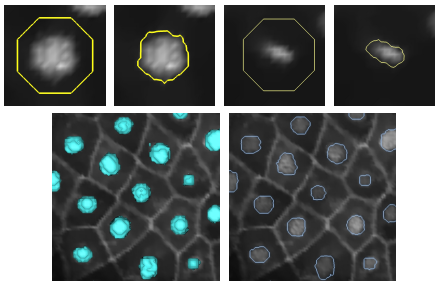

Fig. 4. Cell nuclei segmentation. Top, 2D slice of data with the initial segmentation function and the corresponding segmentation results (isosurface $I = 128$ of the segmentation function). Bottom, the cell image (nuclei and membranes superimposed) with the segmented nuclei. Parameter values $g(s) = G_\rho * 1/(1+Ks^2)^6$, $K = 1000$, $\rho = 0.0001$, $w_a = 10.0$, $w_d = 2.0$, $\tau_S = 0.1$, $h_S = 1.0$, $\varepsilon = 10^{-3}$.

$$D^{pqr-}_{ijk} u = \left( u^{n-1}_{ijk} - u^{n-1}_{i-p,j-q,k-r} \right) / h_S,$$
$$D^{pqr+}_{ijk} u = \left( u^{n-1}_{ijk} - u^{n-1}_{i+p,j+q,k+r} \right) / h_S \qquad (16)$$

and we get

$$\int_{V_{ijk}} w_a \nabla g \cdot \nabla u \, dx \approx w_a h_S^3 \sum_{I_{ijk}} \left( \max \left( D^{pqr}_{ijk} g, 0 \right) D^{pqr-}_{ijk} u + \min \left( D^{pqr}_{ijk} g, 0 \right) D^{pqr+}_{ijk} u \right) \qquad (17)$$

The diffusion term is approximated similarly as in the case of the center detection problem, using the notation (10)

$$\int_{V_{ijk}} w_d \, g |\nabla u^{n-1}| \nabla \cdot \left( \frac{\nabla u^n}{|\nabla u^{n-1}|} \right) dx \approx \qquad (18)$$
$$w_d g_{ijk} h_S \bar{Q}^{n-1}_{ijk} \sum_{N_{ijk}} \frac{u^n_{i+p,j+q,k+r} - u^n_{ijk}}{Q^{pqr;n-1}_{ijk}}.$$

The segmentation that we have described has various interesting applications in the analysis of cell images, cf [1], [14]. The segmentation of any object can be used to determine its volume, surface or evaluate the shape. Moreover, the nuclei segmentation can be used for correction of the center detection, the cell boundary segmentation can be useful in detection of cell divisions. The embryo segmentation together with the center detection can give us the information about the local and global density of cells.

To complete the method description, we provide several illustrative examples displayed in Fig. 4, 5 and 6.

### *D. Extraction of the intercellular skeleton*

The intercellular borders correspond to the ridges of the signed distance function to the segmented inner cell boundaries. The distance function can be computed by numerical solution of the time relaxed eikonal equation

$$d_t + |\nabla d| = 1. \qquad (19)$$

The equation is solved in the domain $\Omega \times [0, T_D]$ and it is coupled with a Dirichlet type condition

$$d(x,t) = 0, \quad x \in \Omega_0 \subset \Omega \qquad (20)$$

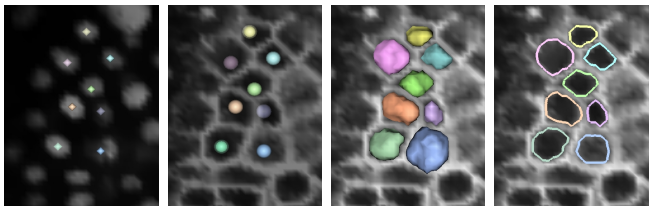

Fig. 5. Segmentation of the inner cell boundaries. From the left: 2D slice of the cell nuclei image with detected centers, 2D slice of the cell membrane image with an isosurface of the initial segmentation function, segmentation results, 2D slice of the segmentation results. Parameters $g(s) = 1/(1+Ks^2)$, $K = 1000$, $w_a = 10.0$, $w_d = 0.2$, $\tau_S = 0.1$, $h_S = 1.0$, $\varepsilon = 10^{-3}$.

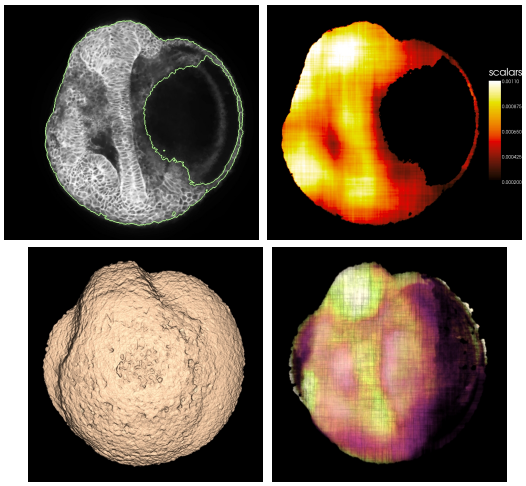


Fig. 6. Embryo surface segmentation and the local cell density. Top left, 2D slice of the segmented embryo surface. Top right, the corresponding distribution of local cell density. Bottom left, segmented surface of the embryo in 3D view. Bottom right, the volume rendering of the local cell density with recongnizable structures. Brighter colors correspond to higher local density. Parameters $g(s) = 1/(1+Ks^2)$, $K = 1000$, $w_a = 10.0$, $w_d = 2.0$, $\tau_S = 0.1$, $h_S = 1.0$, $\varepsilon = 10^{-3}$.

where $\Omega_0$ is the set of curves representing the inner cell borders. Due to the character of the level set function representing the segmentation result, we can recognize the inner and outer parts of the cell. In order to construct the signed distance function $d^\pm$, we set $d^\pm = -d$ inside the cell and $d^\pm = d$ outside.

The time discretization of (19) is explicit and the space discretization is based on the approximation of the center detection model (1) since it has the same structure (if we set $\delta = -1$ and the curvature term is replaced by a constant $f = 1$). The Rouy-Tourin discretization leads to

$$d^n_{ijk} = d^{n-1}_{ijk} + \tau_D - \frac{\tau_D}{h_D} \sqrt{M^{100}_{ijk} + M^{010}_{ijk} + M^{001}_{ijk}}. \qquad (21)$$

The efficiency of this method can be further improved. In [2], a fixing strategy that significantly reduces the CPU time was proposed. This technique takes advantage of the fact that the updates generated by (21) gradually approach a steady state and it updates only the points where the steady state has not been reached yet. We can also realize that we do not necessarily need the exact value of the distance function. What we need is the correct position of the ridges of $d^\pm$ and the

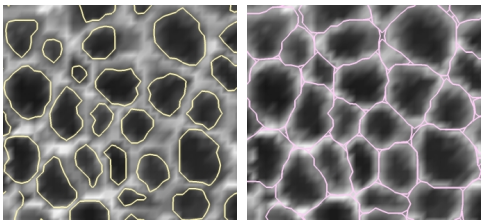

Fig. 7. A detail of the inner cell boundary segmentation (left) with the corresponding segmented intercellular skeleton (right). Parameters $\tau_D = 0.\bar{3}$, $\tau_A = 0.03$, $h_D = h_A = 1.0$.

correct orientation of the vector field generated by the gradient of $d^{\pm}$. This is achieved as soon as all values are non-trivially updated by (21) [2].

The ridges of $d^{\pm}$ are segmented by a simple variant of the generalized subjecctive surface model

$$u_t + \nabla g \cdot \nabla u = 0 \tag{22}$$

where $(x,t) \in \Omega \times [0, T_A]$ and $g(x) = (d^{\pm}(x, T_D))^p$ according to [16] or $g(x) = -1/\left(1 + K\left(d^{\pm}(x,T_D)\right)^p\right)$ with $K > 0$, $p > 0$ as in [13], [10]. The unknown function $u$ is initialized by a piecewise constant profile localized around the approximate cell center. Then it is evolved by (22). The intercellular skeleton is represented by a chosen isosurface of the union of the segmentation results corresponding to the individual cells. For the cells that are in the outer cell layers of the embryo, there is no ridge to stop the evolution of the function $u$ in the parts where there are no neighboring cells. In this case, we use the segmented surface of the embryo to complete the missing boundary.

The equation (22) is discretized using the explicit time approach and the upwind strategy given by (15) and (17). We can write

$$u^n_{ijk} = u^{n-1}_{ijk} - \frac{\tau_A}{h_A} \sum_{I_{ijk}} \Big( \max\left(D^{pqr}_{ijk} g, 0\right) D^{pqr-}_{ijk} u + \min\left(D^{pqr}_{ijk} g, 0\right) D^{pqr+}_{ijk} u \Big) . \tag{23}$$

The intercellular skeleton can be used to determine the area of the cell contact surface. Further, we can evaluate the cell shapes and according to the shape detect specific groups or layers of cells. Having at disposal both inner and outer boundaries of the cells, we can determine the volume occupied by the cell membranes etc. Some examples are shown in Fig. 7, 8.

## III. Conclusion

We described a set of methods designed to segment objects from 3D cell nuclei and cell membrane images. Based on the results, we can conclude that the presented set of methods represents a powerful tool for the analysis of cell images. We mentioned several useful applications that can be further extended within the scope of our future research.

## Acknowledgment

This work was supported by the grants APVV-0351-07, APVV-LPP-0020-07 and the grant of VEGA 1/0269/09.

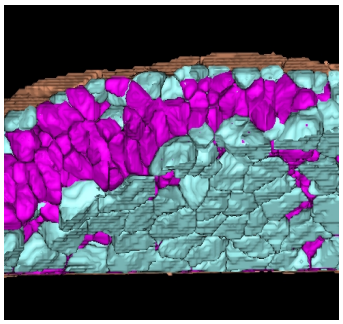

Fig. 8. Differentiated cell layers detected automatically according to the cell shape. The main criterion was the flatness or elongation of the cell and the orientation of the longest side of its bounding box with respect to the normal to the embryo surface.

## References

[1] P. Bourgine, R. Čunderlík, O. Drblíková-Stašová, K. Mikula, N. Peyriéras, M. Remešíková, B. Rizzi, A. Sarti, *4D embryogenesis image analysis using PDE methods of image processing*. Kybernetika 46 (2) (2010).

[2] P. Bourgine, P. Frolkovič, K. Mikula, N. Peyriéras, M. Remešíková, *Extraction of the intercellular skeleton from 2D microscope images of early embryogenesis*. Lecture Notes in Computer Science 5567 (Proceeding of the 2nd International Conference on Scale Space and Variational Methods in Computer Vision, Voss, Norway, June 2009), Springer (2009), 38–49.

[3] M. Campana, B. Maury, P. Dutreix, N. Peyriéras, A. Sarti, *Methods toward in vivo measurement of zebrafish epithelial and deep cell proliferation*. Computer methods and programs in biomedicine, in press (2010).

[4] V. Caselles, R. Kimmel, G. Sapiro, *Geodesic active contours*. International Journal of Computer Vision 22 (1997), 61–79.

[5] Y. Chen, B. C. Vemuri, L. Wang, *Image denoising and segmentation via nonlinear diffusion*. Computers and Mathematics with Applications 39 (2000), 131–149.

[6] S. Corsaro, K. Mikula, A. Sarti, F. Sgallari: Semi-implicit co-volume method in 3D image segmentation. SIAM J. Sci. Comput. 28 (6) (2006), 2248–2265.

[7] P. Frolkovič, K. Mikula, N. Peyrieras, A. Sarti, *A counting number of cells and cell segmentation using advection-diffusion equations*. Kybernetika 43 (6) (2007), 817–829.

[8] S. Kichenassamy, A. Kumar, P. Olver, A. Tannenbaum, A. Yezzi, *Conformal curvature flows: from phase transitions to active vision*. Arch. Rational Mech. Anal. 134 (1996), 275–301.

[9] Z. Krivá, K. Mikula, N. Peyriéras, B. Rizzi, A. Sarti, O.Stašová, *Zebrafish early embryogenesis 3D image filtering by nonlinear partial differential equations*. To appear in Medical Image Analysis (2010).

[10] K. Mikula, N. Peyriéras, M. Remešíková, A. Sarti, *3D embryogenesis image segmentation by the generalized subjective surface method using the finite volume technique*. Proceedings of FVCA5 – 5th International Symposium on Finite Volumes for Complex Applications, Hermes Publ. Paris 2008.

[11] K. Mikula, M. Remešíková, *Finite volume schemes for the generalized subjective surface equation in image segmentation*. Kybernetika 45 (4) (2009).

[12] E. Rouy, A. Tourin, *Viscosity solutions approach to shape-from-shading*. SIAM Journal on Numerical Analysis 29 (3) (1992), 867–884.

[13] A. Sarti, R. Malladi, J. A. Sethian, *Subjective Surfaces: A Method for Completing Missing Boundaries*. Proceedings of the National Academy of Sciences of the United States of America 12 (97) (2000), 6258–6263.

[14] O. Tassy, F. Daian, C. Hudson, V. Bertrandt, P. Lemaire, *A quantitative approach to the study of the cell shapes and interactions during early chordate embryogenesis*. Currrent Biology 16 (2006), 345–358.

[15] C. Zanella, M. Campana, B. Rizzi, C. Melani, G. Sanguinetti, P. Bourgine, K. Mikula, N. Peyriéras, A. Sarti, *Cells Segmentation from 3-D Confocal Images Of Early Zebrafish Embryogenesis*. IEEE Transactions on Image Processing 19 (3), (2010), 770–781.

[16] H.-K. Zhao, S. Osher, R. Fedkiw, *Fast surface reconstruction using the level set method*. Proc. IEEE workshop on variational and level set methods - VLSM'01, Vancouer (2001) 194–201.